Propagating Fronts in Thin Tubes: Concentration, Electric, and pH Effects in a Two-Dimensional Precipitation Pulse System

Rabih Makki,[†] Mazen Al-Ghoul,[†,‡] and Rabih Sultan*[,†]

Department of Chemistry and Center for Advanced Mathematical Sciences, American University of Beirut, P.O. Box 11-0236, 1107 2020 Riad El Solh, Beirut, Lebanon

Received: October 2, 2008; Revised Manuscript Received: April 8, 2009

In this paper, we studied the dynamics of a $CaCO_3$ precipitate deposition pulse in a thin, long tube connecting two reservoir sinks of coprecipitates. The pulse profile, as well as the time t_c and distance x_c of the first appearance of precipitate, is studied as a function of the initial concentration of CO_3^{2-} in the right reservoir, $[CO_3^{2-}]_0$, and later as a function of an applied external electric field at different voltages. The time variations of the pulse location and the pH at the center of the tube are determined. The distance from the calcium chloride sink (x) at any fixed time decreases as $[CO_3^{2-}]_0$ increases. The time evolution of the front location exhibits a crossover between an early time regime and a late time regime. The pH−time curve shows a marked resemblance with a sigmoid shape. At any time, the pH consistently increases with $[CO_3^{2-}]_0$. In the presence of a constant electric field applied across the tube (fixed voltage), t_c decreased with the field strength, whereas x_c exhbited a correlated increase. Irregularities in the variation of distance with the applied voltage (at a fixed time) were noted. The pH experiences a slight increase with the applied voltage. The pulse width exhibits a nonlinear time dependence, of the form $w = a + bt^{1/6}$. The shape of the deposition pulse deviates from a Gaussian distribution. This study is of special interest in the experimental simulation and modeling of precipitate deposition and potential clogging in microcapillary channels.

1. Introduction

A great deal of interest in moving diffusion-reaction fronts of the type A + B → C has been evident, notably in the last two decades. Both experimental[1−7] and theoretical[8−13] approaches have been developed and reported. Front propagation is characterized by interesting end exotic features and governed by a rich dynamics, with significant applications in chemistry,[14,15] biology,[16,17] geology,[18−20] materials science,[21,22] and engineering.[23−25] Of particular interest are those reactions taking place in tubular reactor channels, with reactants being fed by diffusion from separated reservoirs at opposite ends. Two general classes of reactions of that same type and stoichiometry can be distinguished, notably from the viewpoint of the phase of the product (C) defining the reaction front. The first category highlights reaction systems where the product is a 1:1 complex in solution phase. Examples include the Cu^{2+}−tetra,[1,4,6] Cr^{3+}−xylenol orange (XO),[2] and Ca^{2+}−Ca green[5,7] systems. In those reactions, the colored complex makes the front distinctly visible, and the kinetics is thus monitored spectrophotometrically. The experimental studies focus on the width, height, and location of the front, as well as the global reaction rate, along with their time dependence.[4] A crossover between an early irreversible regime and a late reversible regime was demonstrated,[1] and conjectured.[12] The critical scaling exponents were also found to exhibit such a crossover, as predicted by Gálfi and Rácz.[8] Nontrivial crossovers between irreversible regimes along with different classes of universality were reported and conjectured by Taitelbaum and his co-workers.[26,27] Theoretical approaches to the modeling of the A + B → C reaction-diffusion system span scaling ansatz and perturbation techniques,[8,12,26,27] mean-field theory[4,10] as well as Monte Carlo[9] and other numerical methods.[2,5,11,13]

The second class groups reactions where the product C is a solid, and hence the moving front is located at the solid−solution interface. When one ionic diffusion source is present, invading an immobile phase (gel) containing a coprecipitate ion, a uniform precipitation front is formed, or more typically, Liesegang bands.[28−30] In this study, we direct our interest at precipitation fronts in tubular reactor systems where the coprecipitate ions diffuse from separate reservoirs at opposite ends. López Cabarcos et al.[3] studied the propagation of a $CaHPO_4$ deposit in an agarose gel channel from Ca^{2+} and HPO_4^{2-}, initially separated as just described. They established that a crossover between a spatially uniform pulse and a pattern of periodic bands is observed as the concentration gradient increases through zero. The scaling laws for the time of formation of the precipitate as well as its width were determined. For a zero gradient, the deposit zone became narrower as the concentration of reactants increased. Marek, Pribyl, and their co-workers,[13] whose paper lies at the basis of the motivation for this study, theoretically studied the effect of electric field on the evolution of a calcium carbonate deposit in a 1D system, fed by $CaCl_2$ and Na_2CO_3 sources. The authors showed that the application of an electric field caused precipitation to occur faster and in a much broader range of electrolyte concentrations than in the case without the imposed field; hence the possibility of microsystem clogging was shown to increase. Peak splitting was also obtained in dependence on the applied field strength and attributed to the formation of a steep gradient of electric potential within the microcapillary. Pribyl et al.[13] noted that the interest in microtechnology and nanotechnology in the past decade has instigated an intensive research on the electrokinetic phenomena in microstructures, particularly the effect of electric

* Corresponding author. rsultan@aub.edu.lb.
[†] Department of Chemistry.
[‡] Center for Advanced Mathematical Sciences.

10.1021/jp8087226 CCC: $40.75
Published on Web 05/01/2009

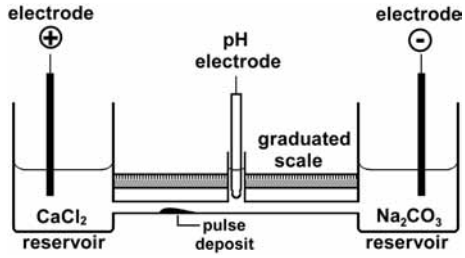

Figure 1. Experimental setup.

fields on the processes inside microcapillaries and more complex microstructures.

In the present study, we verify experimentally some results obtained by the theoretical study of Marek, Pribyl, and their co-workers.[13] The setup consists of two reservoirs containing aqueous electrolytes of sodium carbonate and calcium chloride, connected by a thin tube containing distilled water. As the calcium and carbonate ions interdiffuse and migrate in the tube, calcium carbonate precipitates whenever and wherever the concentration product of the calcium and carbonate ions exceeds the $CaCO_3$ solubility product.

Two major effects on the reaction-transport processes will be investigated: the concentration of CO_3^{2-} ion in the right reservoir $[CO_3^{2-}]_0$ (while the concentration of Ca^{2+} in the left reservoir is kept constant) and the strength of a constant electric field applied across the tube. The spatial profile of the precipitate pulse and its time evolution will be studied, and the location of the leading edge of the traveling precipitate pulse will be measured with time. The pH of the solution in the middle of the tube will also be monitored as a function of the various system parameters. The system is expected to exhibit a pH dependence, since the carbonate system is governed by the following H^+ equilibrium reactions

$$H_2CO_3(aq) \rightleftharpoons H^+(aq) + HCO_3^-(aq) \quad (1)$$

$$HCO_3^-(aq) \rightleftharpoons H^+(aq) + CO_3^{2-}(aq) \quad (2)$$

$$H_2O(l) \rightleftharpoons H^+(aq) + OH^-(aq) \quad (3)$$

The observations and results will be discussed in conjunction with the reaction-transport processes involved and in relation with problems of clogging and capillary flow dynamics.

2. Experimental Section

2.1. Setup. The block diagram of the experimental setup, shown in Figure 1, consists of two 400 mL beakers connected by a thin tube of length 40.0 cm and internal diameter 4.0 mm. Although the length-to-diameter ratio is relatively large (100), this long tube system still simulates a 2D pulse in space, by virtue of the significance of its height span, along with its spatial structure. The tube has an opening in its middle, which enables us to immerse a pH electrode (Orion 8102 BNU), to measure the pH in that region (using an Orion 550A pH-meter), at different time intervals during the experiment. In some experiments, an electric potential difference between the two reservoirs is applied, using a dc power supply (LG, GP-4303D) connected to stainless steel electrodes placed at the center of each beaker. The electrodes consist of plates made of steel of length 15 cm and width 3 cm, separated by a distance of 48 cm. The electrode composition is summarized in Table 1. The distance x between the front edge of the $CaCO_3$ precipitate pulse and the $CaCl_2$ beaker (taken as a measure of the pulse location) is measured manually with a fixed ruler, and pictures are taken with a digital camera (Sony, DSC-F828) and transformed into black and white using an appropriate threshold with Corel Photo-Paint.

TABLE 1: The Composition of the Stainless Steel Electrodes (% by mass)

	Fe	Cr	Ni	Mo	Mn	Si	C	P	S
mass %	68.845	16	10	2	2	1	0.08	0.045	0.03

TABLE 2: Initial Concentrations of $CaCl_2$ and Na_2CO_3 (obtained by instant dilution of solutions A and B, respectively)

$[CaCl_2]_0$ (M)	$[Na_2CO_3]_0$ (M)
0.100	0.100
0.100	0.150
0.100	0.200
0.100	0.250

2.2. Procedure. First, standard solutions are prepared with concentrations four times greater than those desired at the start of the experiment (call **A**, the concentrated $CaCl_2$ solution, and **B** the concentrated Na_2CO_3 solution). They are diluted by an instantaneous mixing with water right at the moment marking time $t = 0$, to designate the initial concentrations in the right and left reservoirs. The initial concentration of sodium carbonate in the right reservoir, $[Na_2CO_3]_0$, is varied in the range between 0.100 and 0.250 M, while the initial concentration of calcium chloride in the left reservoir is kept constant ($[CaCl_2]_0 = 0.100$ M). The resulting initial concentrations of the starting solutions are summarized in Table 2.

One hundred fifty milliliters of double distilled water is added to each of two 400 mL beakers connected by a thin tube. An additional 7.66 mL of double distilled water is also added to one of the beakers to make up for the water volume lost in the tube. A pH combination electrode is immersed in a special cylindrical cavity at the middle of the tube and connected to a pH-meter (see Figure 1). The pH-meter is subjected to a three-point calibration, using three buffers (7.00, 4.01, and 10.01). Temperature control (±1 °C) is achieved by placing the whole apparatus in an air thermostat. When the setup is ready, 50.0 mL of solution **A** is poured into the left beaker and 50.0 mL of solution **B** is poured into the right beaker at exactly the same time. This instant marks $t = 0$, at which the chronometer is started.

It is to be noted that the reaction was run without stirring of the reservoirs, as the medium would experience streaming currents. The latter would enhance advection in an uncontrollable way, and this was actually found to significantly alter the observed dynamics and cause a deformation of the pulse profile. Furthermore the role of CO_2 from the air was assumed to be negligible. This assumption is justified on the account of the relatively large CO_3^{2-} concentrations used and the fact that CO_3^{2-} (not HCO_3^-) was notably the reactant, which renders the role of CO_2 strictly minimal since for H_2CO_3 $K_1/K_2 = 9.6 \times 10^3$.[31]

In experiments involving an electric field, stainless steel electrodes are immersed at the center of each solution (in the reservoir beakers), separated by a distance of 48 cm. We assume that the minor amounts of side products due to the electrode reactions do not affect the transport and chemical processes taking place inside the thin tube.

When the precipitate starts to appear, the distance of the front edge of the precipitate from the $CaCl_2$ beaker (call it x) is measured manually with a fixed graduated scale to the nearest 0.05 cm, and pictures are taken with a digital camera at time intervals of 20−30 min. The pH at the center of the tube is

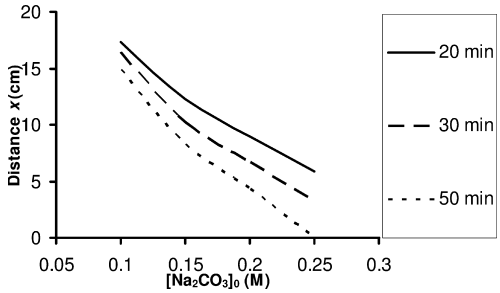

Figure 2. Distance vs $[Na_2CO_3]_0$, at fixed $[CaCl_2]_0 = 0.100$ M and at times indicated in the legend. The distance is measured from the Ca^{2+} reservoir to the edge of the precipitate pulse. Time is measured from the instant of the addition of the reagents.

measured periodically, for about 5 consecutive hours. The initial concentration of CO_3^{2-} in the right reservoir ($[CO_3^{2-}]_0$) and the potential difference applied between the two beakers are varied over various sets of runs. Each experiment (at a given concentration and potential difference) is performed in duplicate or triplicate to test the reproducibility and record average measurements. The time (t_c) and distance (x_c) of the first appearance of the precipitate are measured and plotted with varying $[CO_3^{2-}]_0$ and voltage.

3. Concentration Effects

As described earlier, we investigate the effect of varying the initial concentration of CO_3^{2-} on the system properties, while the initial concentration of Ca^{2+} is kept constant. The properties monitored here are mainly the pulse propagation and the pH variation. No electric field is applied in this section.

3.1. Pulse Propagation. The variation of the location of the precipitate pulse (plotted as the distance x) with the initial sodium carbonate concentration, $[Na_2CO_3]_0$, at three different times is depicted in Figure 2.

The plots indicate that the distance x always decreases as $[Na_2CO_3]_0$ increases at all the given times. Indeed, as $[Na_2CO_3]_0$ increases, the larger gradient drives the diffusion faster, thus rendering the overall diffusion-deposition front faster. Hence at a given time, the distance traveled at higher $[Na_2CO_3]_0$ is greater, that is, distance to the Ca^{2+} reservoir is less and, hence, decreases with $[CO_3^{2-}]_0$. Furthermore, for all $[Na_2CO_3]_0$ concentrations, the distance always decreases as time increases; that is, the higher time curves lie below the lower ones. This is due to the fact that $[CO_3^{2-}]_0$ in the above experiments is always greater than or equal to $[Ca^{2+}]_0$. This implies a net diffusion toward the Ca^{2+} compartment (down the larger CO_3^{2-} gradient); hence the front advances toward the latter compartment. It is also noteworthy to point out that the diffusion coefficient of carbonate ions ($D_{CO_3^{2-}} = 8.0 \times 10^{-10}$ m^2 s^{-1}) is greater than that of calcium ions ($D_{Ca^{2+}} = 7.0 \times 10^{-10}$ m^2 s^{-1}). This result was also observed by Kobe,[32] who noted that the species with the higher diffusion coefficient will diffuse further and the species with the larger initial concentration will diffuse faster due to the large gradient it experiences.

To visualize the deposition pulse profile, digital photographs of the pulse in the tube are taken using a SONY digital camera (Sony, DSC-F828), and transformed into black and white using a suitable threshold, by means of the software Corel Photo-Paint. The resulting pulse profiles are then mapped onto a 2D spatial representation displaying the height and the width of the precipitate zone. Figure 3 displays the shape of the pulse profile (edge located at x) at three different concentrations $[Na_2CO_3]_0$, at a constant time ($t = 15$ min). The $[Na_2CO_3]_0 =$

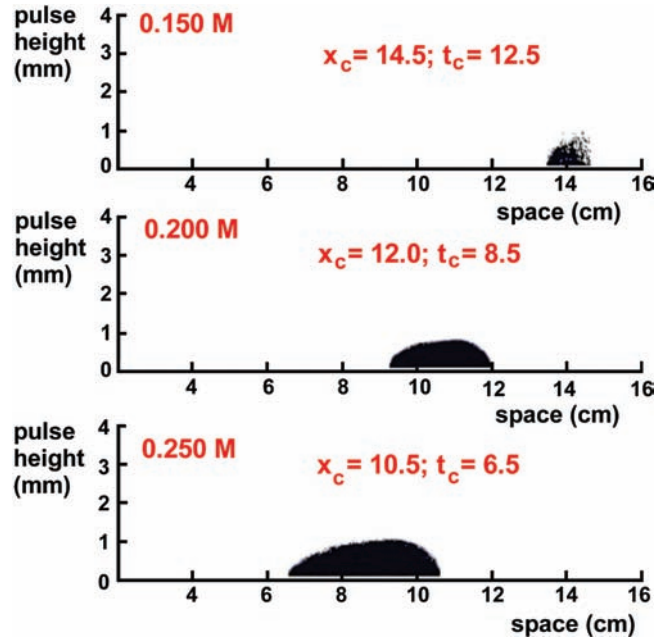

Figure 3. Appearance of a pulse profile of $CaCO_3$ deposit at a fixed time ($t = 15$ min) at different sodium carbonate initial concentrations, $[Na_2CO_3]_0$, indicated on the figure, for a fixed $[CaCl_2]_0 = 0.100$ M. The time (t_c) and distance (x_c) of appearance of the pulse deposit are marked on the figure, for each concentration.

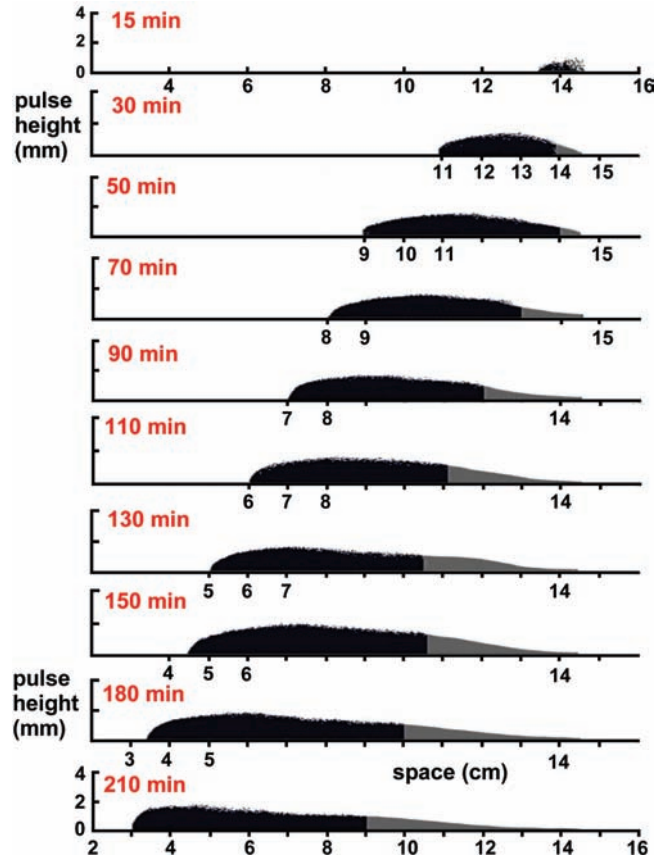

Figure 4. Time evolution of the pulse profile. The image is equivalent to a 2D cross section, of a height and width as shown. $[CaCl_2]_0 = 0.100$ M, $[Na_2CO_3]_0 = 0.150$ M.

0.100 M profile does not appear in the plot, because the critical time for its first appearance (t_c) >15 min. In Figure 4, the time evolution of the precipitate deposition pulse is monitored and highlighted (for an experiment wherein $[CaCl_2]_0 = 0.100$ M,

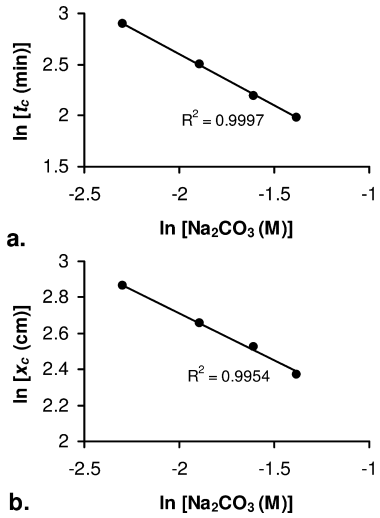

Figure 5. (a) log−log plot of t_c vs $[Na_2CO_3]_0$; slope = −1.013. (b) log−log plot of x_c vs $[Na_2CO_3]_0$; slope = −0.525. Both plots exhibit a linear dependence, in conformity with the power law. $[CaCl_2]_0$ = 0.100 M.

$[Na_2CO_3]_0$ = 0.150 M, t_c = 12.5 min, and x_c = 14.50 cm). Given that in some cases (at long times) the pictures span only a small portion of the deposit to avoid Parallax error, the tail of the pulse is drawn by extrapolation in gray.

The parameters t_c and x_c, which are defined as the time and the distance of the first appearance of the precipitate, respectively, are studied as functions of $[Na_2CO_3]_0$. The (natural) log−log dependence of t_c and x_c on $[CO_3^{2-}]_0$ is shown in Figure 5 (at fixed $[Ca^{2+}]_0$ = 0.100 M). We see that the latter dependence exhibits an almost perfect linearity (R^2 = 0.9997 and 0.9954, respectively), in conformity with the power law. López-Cabarcos et al.[3] obtained a similar relation for the formation time of $CaHPO_4$ in agarose gel, but with less marked linearity. In their study, the width of the front also obeyed the power law, with a clear decrease with concentration, used equally for the electrolytes at both ends, thus with a zero concentration difference. Under conditions where unequal concentrations were used,[3] Liesegang bands were obtained, a situation not encountered in the present study under any of the working conditions. Furthermore, as expected, both t_c and x_c decrease as $[Na_2CO_3]_0$ increases. As the concentration of the diffusing coprecipitating ions increases, the time needed to exceed the solubility product in the tube will be shorter. x_c decreases since as $[Na_2CO_3]_0$ increases, the larger gradient drives the diffusion faster. Hence at a given time, the distance traveled at higher $[Na_2CO_3]_0$ is greater, that is, the distance x (to the Ca^{2+} reservoir) is less. This result was compared and found to agree with the theoretical results of Pribyl et al.[13] who established that t_c decreases as $[CO_3^{2-}]_0$ increases (especially at low carbonate concentrations), while x_c also decreases but slightly with an increase in $[CO_3^{2-}]_0$. In their paper, they display x_c and t_c versus concentration but do not show the log−log plot. However the slopes can be easily extracted from Figure 4 of Pribyl's paper. The plots of ln t_c and ln x_c versus ln c yield average slopes of − 0.23 and − 0.060, respectively, whereas in our work the slopes are −1.013 and −0.525 (see Figure 5 and its caption). Thus, the slopes of Pribyl et al.[13] are 1 order of magnitude lower than ours. We can generally estimate the time scale for diffusion of a species by the relation L^2/D. Thus, for a length of 1 cm and a typical diffusion coefficient for an ion in water of 10^{-9} m^2 s^{-1}, the time scale would be of the order of 10^5 s. Since our critical time t_c is of the order of minutes,

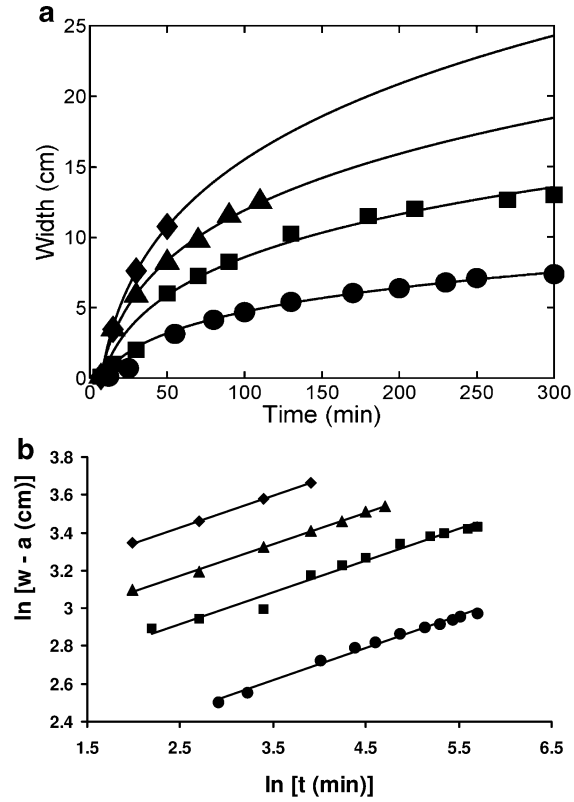

Figure 6. (a) Variation of the pulse width with time t at fixed $[Ca^{2+}]_0$ = 0.100 M, and different $[Na_2CO_3]_0$ values. $[CO_3^{2-}]_0$: ●, 0.100 M; ■, 0.150 M; ▲, 0.200 M; ◆, 0.250 M. The lines show curve fit trend lines, with equation of the form $w = a + bt^{1/6}$. (b) log−log plots for the curves in (a), of equal slope = 1/6.

we can infer that advection plays an important role in our experiments, notably that the tubular reactor is gel free. This advection effect is mostly caused by the initial mixing and eases tremendously after a certain time beyond which diffusion becomes dominant, as we observed in separate tests on the propagation of a $KMnO_4$ front, from a solution poured under exactly similar conditions. Because a tiny fraction of the ions is needed to migrate to the middle of the tube for the solubility product to be exceeded, the advection effect seems to tremendously decrease the value of t_c. An interesting feature here is that in addition to the different length scales between our system and Pribyl's model (40 cm compared with 1 mm), the presence of advection could well be another factor causing the 1 order of magnitude discrepancy between our experimental results and the theoretical slopes of Pribyl et al., wherein only diffusion is included in the model. Theoretical models of reaction-diffusion-advection processes in tubular reactors, along with experimental studies were developed[33,34] and shown to significantly alter power laws.[34]

Figure 6a shows the temporal variation of the pulse width (w) obtained here, plotted at four different $[CO_3^{2-}]_0$ at constant $[Ca^{2+}]_0$ concentrations. The four plots were then fitted into curves obeying the equation $w = a + bt^{1/6}$, where a and b are fitting parameters. It was found that the relation $w = a + bt^{1/6}$ was near perfectly obeyed, thus reproducing previous results on the time dependence of the front width in chemical reactions of the general form A + B → C.[35] The log−log variation of the quantity ($w - a$) with time, depicted in Figure 6b, reveals an excellent fit of the power law, with slope = 1/6. Furthermore, the width increases with increasing concentration difference. Thus, the nonzero concentration difference plays an important role in altering the dynamics of the system. The precipitation

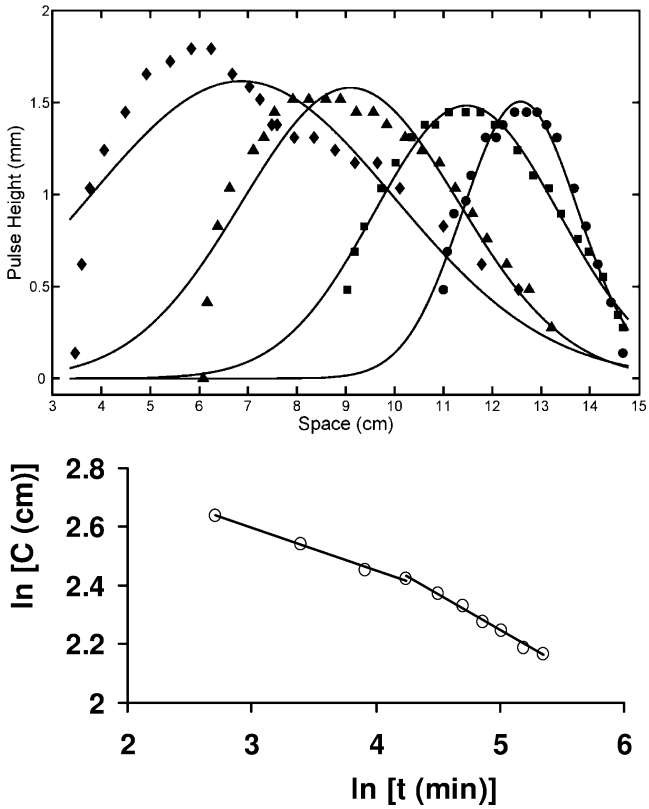

Figure 7. (a) Curve fits of the profile of the deposition pulse for the experiment in Figure 4 ($[CaCl_2]_0 = 0.100$ M, $[Na_2CO_3]_0 = 0.150$ M). The chosen times are, from right to left: 30, 50, 110, 180 min. (b) log−log plots for the location of the center of the pulse (C) with time t. The power law shows a crossover between an early time and a late time regimes. The slope of the log−log plot changes from −0.14 to −0.25.

profile in ref 3 resembles a Gaussian shape, a behavior not reproduced here (see notably Figure 4). A closer look at the shape of the deposition profiles obtained here reveals a clear deviation from a Gaussian distribution. Figure 7a displays curve fits of the deposition profiles. We see that the leading edge of the pulse drops suddenly beyond a sharp cusp at the precipitation sink (as previously remarked in the profiles of Figure 4), breaking the smoothness of the diffusion profile. This certainly presents an interesting variant from known front shapes[3,35] and Liesegang bands.[36,37] The front shapes in the former, and the particle size distribution in the latter essentially obey Gaussian fits. In Figure 7b, we display the log−log plot for the center (C) of the pulse profiles of Figure 4 versus time. The plot exhibits a linear appearance, however, with a crossover between early and late times (slopes −0.14 and −0.25, respectively). We see that the diffusive square root form is not strictly obeyed, unless we assume that the increasing power law exponent eventually tends to the value −1/2 in the limit of very long time. On another note, the obtained crossover result is particularly interesting, as it captures the features of front propagation in a number of studied chemical reaction systems.[1,8,12,26,27] The values 0.14 and 0.25 have an intrinsic significance in that they seemingly fit the fractional exponents 1/6 and 1/4, respectively. The crossover obtained here resembles to a great extent the results of Havlin et al.[38,39] for the dimensionality study of the diffusion-controlled reaction A + B → C. They found that the power law exponent α for the pulse width experiences a transition between ∼0.3 and 1/6, corresponding to a crossover between 1D and mean-field length scales, respectively. This similarity is of notable relevance, given that the relative

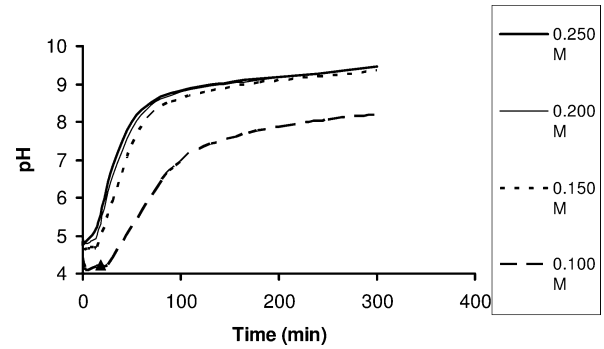

Figure 8. pH vs time, with $[CaCl_2]_0 = 0.100$ M, at various $[Na_2CO_3]_0$, each with curve designation indicated in the legend.

dimensions of our tube are quasi-1D, especially at short time ($\alpha = 0.25$), when the pulse height is slim. A crossover between a simple power law with $\alpha = 1/4$, and one with a logarithmic correction of the form $t^{1/6}(\ln t)^{1/3}$ was also found in the transition between 1D and 2D, for the front width in a diffusion-limited annihilation system of the form A + B → ∅.[40] The value of 1/4 for α was attained for an A + B → C reaction-diffusion front conjectured in a 1D regime with disordered spatial confinement;[41] consistently, it was also obtained in the probability density function treatment of a 1D trapping problem (A + B → B).[42] In a reaction-diffusion system with reactants (Ca^{2+}−Ca green) initially separated by a semipermeable membrane, Park et al.[7] observed a dynamical transition of the front characteristics between several time regimes: an early time, an intermediate time, and an asymptotic time regime. The crossover times between those regimes were found to depend on the membrane thickness. Gálfi and Rácz[8] carried out an analytical calculation of the precipitate front properties, through the coupling of diffusion to the second-order reaction kinetics (A + B → C). They found that the distance traveled by the front scales as $t^{1/2}$, while the pulse width scales as $t^{1/6}$ and the rate of product formation as $t^{-2/3}$. Using scaling perturbation techniques, Taitelbaum et al.[26,27] found various time dependences of the reaction center as a function of the ratio of diffusion coefficients and ratio of initial concentrations of the reacting species. They noted different crossovers with transient scaling exponents of 1/2 (short times) and 3/2 (intermediate times) before reaching the asympmtotic regime of 1/2. In some cases, extrema in the time evolution of the reaction center at intermediate times were theoretically predicted and confirmed experimentally.[27] In the present work, it is interesting to see that whereas the width time dependence is captured here ($t^{1/6}$), the diffusive square root form is not satisfied.

3.2. pH Variation. As mentioned before, the pH was measured in the middle of the reaction tube at regular time intervals, by means of a pH electrode. Figure 8 shows the time variation of the pH for different initial sodium carbonate concentrations.

The initial pH value (around 5) is expected since the double distilled water in the experiment was not deionized (CO_2 from the air dissolves to form carbonic acid, hence lowering the pH of distilled water). Immediately after the reagents are poured in the reservoirs (marking instant $t = 0$), the central region pH experiences a little drift downward, as seen in the slight decrease near $t = 0$. This is essentially caused by a sudden advection stream induced by the initial forced mixing, which resulted in an additional streaming potential. Slightly after the drift, the pH exhibits a slow increase for a short time and then grows more abruptly, passes through an inflection point, and then

continues toward what appears to be a plateau, just like a sigmoidal curve. Three important realizations can be deduced from the pH−time curves:

(1) The pH increases gradually, in parallel with a gradual invasion of the tube domain by CO_3^{2-}, which causes a release of OH^-, by virtue of the reaction

$$CO_3^{2-}(aq) + H_2O(l) \rightleftharpoons OH^-(aq) + HCO_3^-(aq)$$

(2) The pH of the system seems to be insensitive to the start of precipitation, and the subsequent front propagation stages (t_c is marked by the small triangle in Figure 8). This is due to the continuous replenishment with CO_3^{2-} from the right reservoir.

(3) The last stage flattening (tending toward a plateau) is governed by the smoothening of the diffusion profiles.

As shown in Figure 8, the pH slightly increases as $[Na_2CO_3]_0$ increases, with a fairly big gap existing between the 0.100 and 0.150 M cases. This is because a higher $[Na_2CO_3]_0$ is a larger source of OH^- as discussed earlier. This result is in good agreement with the theoretical predictions of Pribyl et al.[13] who established that a high concentration of the carbonate and the bicarbonate ions in the reaction system enhances their association reactions with H^+, which results in an increase of the mean pH value in the tube.

Note that we did not investigate the effect of pH variation on the reaction front and the deposition pulse. Because the carbonate ion is sensitive to H^+ equilibria (reactions 1−3), we would expect the reaction front to exhibit a pH dependence. The effect of the reaction itself on the pH of the solution is rather monitored here and only at the tube center because of technical difficulty. A setup for measuring pH profiles in space is under current construction. The pH−time curves are hence essentially governed by $[CO_3^{2-}]$ (t). Note that in all the concentration runs of Figure 8, the CO_3^{2-} front had already crossed the middle of the tube and the precipitation had occurred at a relatively early time. The sharp rise marks the crossing of the front. In other reaction systems of the type A + B → C, the pH dependence is marked by the number of ionic forms (tautomers) of the ligand. In ref 2, the ligand (XO) has 10 possible tautomers and the degree of aggregation is thus highly dependent on pH.

4. Electric Field Effects

The effect of a constant electric field applied across the tubular medium on the system dynamics is now investigated. Both the initial concentration of sodium carbonate, $[Na_2CO_3]_0$, and the electric field strength are varied while the initial concentration of calcium chloride $[CaCl_2]_0$ is kept constant ($[CaCl_2]_0 = 0.100$ M), at a temperature of 20 ± 1 °C maintained constant inside an air thermostat. The $[Na_2CO_3]_0$ is varied in the range between 0.100 and 0.250 M, while the applied voltage ranges between 0 and 15.0 V. The electrodes are placed at the centers of the beakers, separated by a distance of 48 cm; the field is turned on at the very instant of addition of the reagents, i.e., at $t = 0$.

4.1. Pulse Propagation. The variation of distance with voltage for the different $[Na_2CO_3]_0$ concentrations did not follow a general, well-defined trend. Figure 9a shows the variation of distance x with time at different applied voltages. Figure 9b shows the variation of distance x with voltage at a specific time ($t = 15$ min) for $[CO_3^{2-}]_0 = 0.250$ M, and $[Ca^{2+}]_0 = 0.100$ M. The oscillation shown in Figure 9b is not reproduced in the same way at different times, revealing the higher complexity in those electric field experiments. The same problem was encountered in other runs with different sets of initial concentrations, wherein the distance−time−voltage dependence could not be explicitly determined. This reveals a complex nonlinear behavior of this reaction−transport system in the presence of the field.

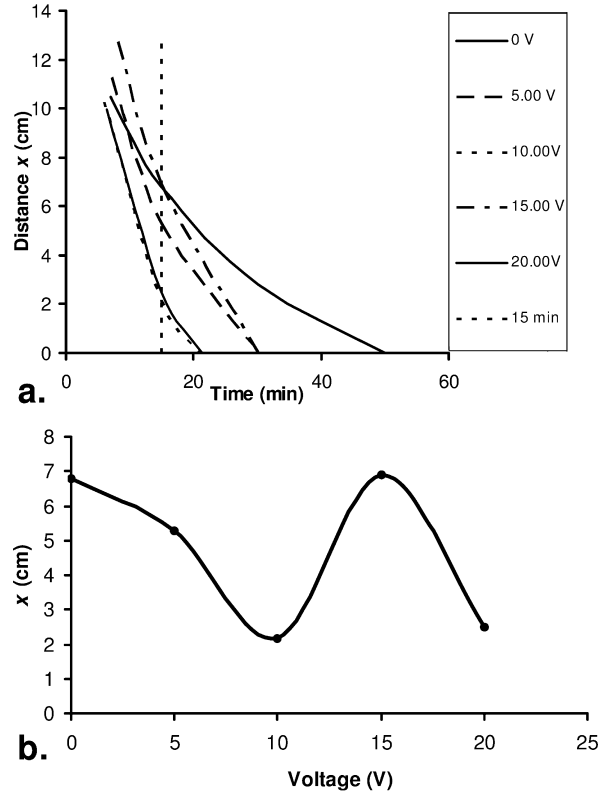

Figure 9. (a) Distance vs time at different voltages (values in the legend), (b) Variation of the front position with voltage at a chosen time $t = 15$ min. $[Na_2CO_3]_0 = 0.250$ M; $[CaCl_2]_0 = 0.100$ M.

Pulse profiles showing the variation of the leading edge location with voltage (for fixed $[Na_2CO_3]_0 = 0.150$ M, $[CaCl_2]_0 = 0.100$ M) at a fixed time ($t = 50$ min) are highlighted in Figure 10.

The effect of varying the electric field strength on the critical time t_c, and the critical distance x_c, for each $[Na_2CO_3]_0$ is depicted in Figure 11. We note here that the electromigration of Ca^{2+} and its diffusive flux are coupled in the same direction (negative electrode in the CO_3^{2-} compartment), and the same applies for CO_3^{2-}. This favored coupling in the presence of the field causes the encounter and the precipitation to occur earlier. The solubility product of calcium carbonate (K_{sp}) can thus be exceeded earlier in the thin tube. Indeed, as shown in Figure 11a, for each $[Na_2CO_3]_0$, t_c decreases as the voltage increases (notably for $[Na_2CO_3]_0 = 0.100$ M). This result agrees with the theoretical findings of Pribyl et al.,[13] who determined that t_c decreases as the applied voltage between the two compartments is increased. It is also in harmony with the experimental evidence that the presence of casual electric effects promotes clogging in piping systems, a problem of significant importance in industrial applications. The electric field enhances the collision between ions, such as Ca^{2+} and CO_3^{2-}, thus increasing the chances of ion combination and subsequent bulk precipitation.

Similarly, Figure 11b shows that x_c slightly increases with the applied voltage. Although the point (0.250 M, 10.00 V) seems to be an exception, the trend can be considered satisfactory at all voltages and concentrations. This result was also found to agree with Pribyl et al.,[13] who established that x_c slightly increases with the applied voltage before peak splitting starts

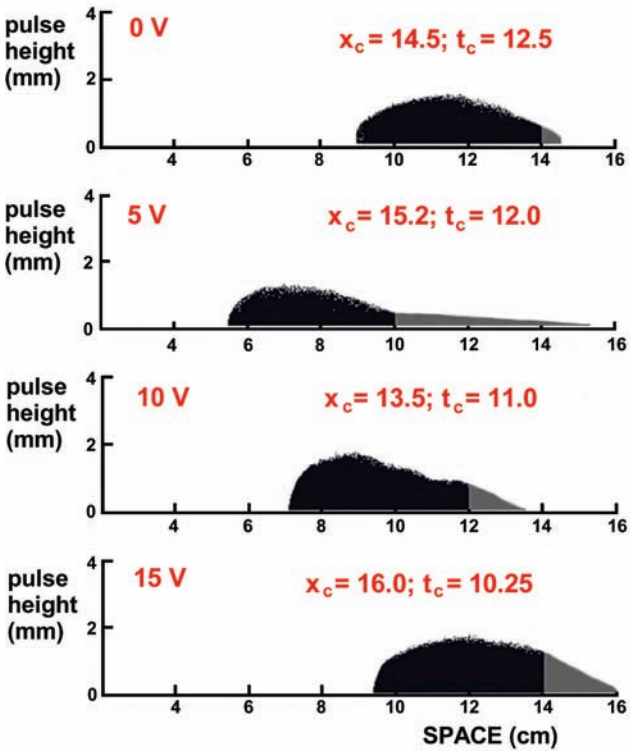

Figure 10. Pulse profile shapes of the $CaCO_3$ deposit at a fixed time (t = 50 min), for fixed initial concentrations of $[CaCl_2]_0$ = 0.100 M and $[Na_2CO_3]_0$ = 0.150 M. The four frames represent four different applied voltages. No specific comprehensible trend could be extracted.

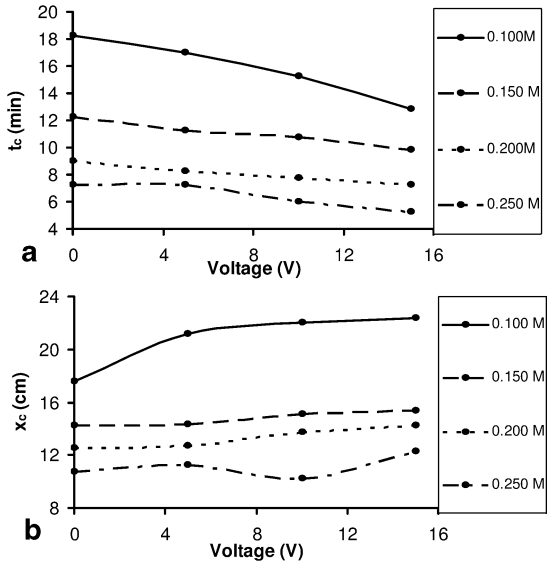

Figure 11. Effect of varying the electric field strength on the critical time, t_c, and the critical distance, x_c, for different $[Na_2CO_3]_0$ values, depicted in the legend. (a) Plot of t_c vs voltage. (b) Plot of x_c vs voltage. In both cases, $[CaCl_2]_0$ is kept constant at 0.100 M.

to occur (<1 V). The latter peak splitting was not detected here, most probably due to low field strengths used (a maximum of 31 V m^{-1}, as compared with 10^3 V m^{-1} in Pribyl's work).

The increase in x_c and the decrease in t_c are clearly correlated. An earlier appearance of the precipitate pulse (lower t_c value) is in congruence with its formation farther away from the reference point (the $CaCl_2$ beaker), i.e., at a higher x_c value. A pertinent question to be asked here is how then can we explain

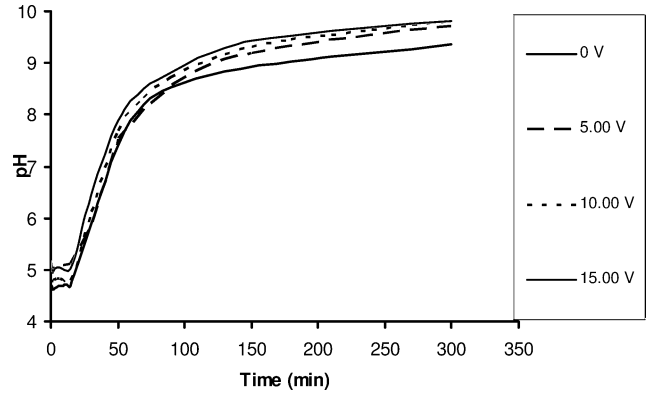

Figure 12. pH vs time, at fixed $[Na_2CO_3]_0$ = 0.150 M and $[CaCl_2]_0$ = 0.100 M. The applied voltage for each plot is highlighted in the legend.

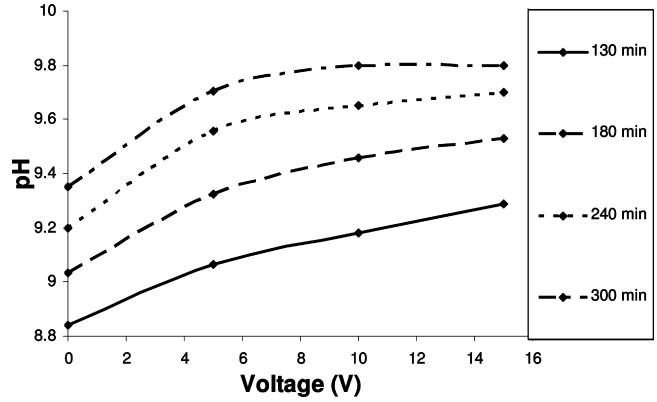

Figure 13. pH vs voltage, at fixed $[Na_2CO_3]_0$ = 0.150 M and $[CaCl_2]_0$ = 0.100 M. The time in minutes for each plot appears in the legend.

the subsequent erratic trend in the distance versus time plots, although the trend of x_c variation with the voltage is well-defined?

It is clear that the effect of the electric field on the electromigration of the ions is rigorous and is reflected in the anticorrelated variation (opposite trends) of x_c and t_c. The pulse propagation along with its 3D texture and morphological alterations seem however to be sensitive to the electric field, in an unpredictable way. Hence the erratic accumulation of the particles in the tube and their remodeling by small streaming effects appear to couple to the added electric effects, due to possible interactions between the electrolyte and excess charge on the precipitate surface caused by ion adsorption.[43,22] Clearly this influences the distance−time variation of the deposit in the presence of the field, after the birth of the pulse and has no effect on the trends of x_c and t_c.

Front propagation in reaction (A + B → C)−diffusion systems in the presence of an electric field was notably studied by Bena and co-workers.[44] They derived equations for the concentration profile of product C in space. They found a linear dependence on the spatial variable x in the case of a positive field (applied in the direction of propagation) and a nonlinear relation in the case of a negative (reverse) field.

4.2. pH Variation. The effect of varying the electric field strength on pH for $[Na_2CO_3]_0$ = 0.150 M is summarized in Figures 12 and 13.

In Figure 12 the pH increases with time at fixed potential difference in a sigmoidal fashion, just resembling the field-free behavior. We further see that the higher voltage curves lie above the lower voltage ones (Figure 12), implying a smooth increase

of pH with voltage at a fixed time. This is also illustrated in the variation of pH with voltage plotted at different constant times, in Figure 13. Thus, the pH slightly and smoothly increases as the potential difference between the Ca^{2+} and CO_3^{2-} compartments increases at a specific time. When a potential difference is applied, and if advection is ignored, mass transport is coupled through diffusion and electromigration to the chemical reactions involved according to the equation

$$\frac{\partial c}{\partial t} = D\frac{\partial^2 c}{\partial x^2} - v\frac{\partial c}{\partial x} + F(c)$$

where D is the diffusion coefficient, v is the magnitude of the field vector (here proportional to the electric field strength), and $F(c)$ is a chemical reaction rate law. Note that CO_3^{2-} is the net diffusing species ($[Ca^{2+}]_0 \leq [CO_3^{2-}]_0$); hence diffusion will be enhanced by the electric field since the positive electrode is in the Ca^{2+} compartment (CO_3^{2-} migrates toward the positive electrode, resulting in a positive feedback coupling to the gradient). As a consequence, $[CO_3^{2-}]$ at time t in the middle of the thin tube will be larger at higher applied voltages, which is reflected in an increase in the pH. A similar effect for pH variation with the electric field is observed with all the other $[Na_2CO_3]_0$ concentrations tested, but they are not shown here for simplicity. Finally, we note that comparison of our results with the theoretical findings of Pribyl et al.,[13] though qualitatively sound, suffers from differences in the length and electric field strength scales, as well as the role of advection in our gel-free reactor.

5. Conclusions, Discussion, and Applications

The main findings of the present study may now be summarized as follows:

(1) The distance of the precipitate pulse from the $CaCl_2$ beaker always decreases with time (the pulse advances toward the $CaCl_2$ beaker), and it decreases as $[Na_2CO_3]_0$ increases at constant $[CaCl_2]_0$.

(2) The critical time t_c, and the critical distance x_c decrease as $[Na_2CO_3]_0$ increases at constant $[CaCl_2]_0$. The log−log plots of the latter variations are linear, with slopes −1.013 and −0.525, respectively. These slopes are 1 order of magnitude higher than those obtained by Pribyl et al.[13]

(3) The pulse width (w) exhibits a nonlinear time dependence, of the form $w = a + bt^{1/6}$.

(4) The shape of the deposition pulse deviates from a Gaussian distribution.

(5) The pH at the center of the tube increases with $[Na_2CO_3]_0$ at constant $[CaCl_2]_0$.

(6) The same trends for the pH variation and pulse propagation are obtained under an applied constant electric field, both in time and as the initial concentration $[Na_2CO_3]_0$ is varied.

(7) The pH slightly increases as the potential difference between the Ca^{2+} and CO_3^{2-} compartments increases at a specific time.

(8) The variation of the distance with applied voltage is irregular in the sense that the distance−time curves at different voltages (fixed $[Na_2CO_3]_0$) alternate and cross in an irregular way.

(9) The critical time, t_c, decreases as the applied voltage increases, whereas the critical distance, x_c, increases with increasing voltage.

In addition to its relevance in the area of diffusion−precipitation reactions, this study could find potential use and application in industrial engineering, wherein the phenomenon of clogging creates a major problem in that it shortens the lifetime of heat exchangers and deteriorates the performance of highly expensive process equipment.[23] Clogging (or fouling) is viewed as the accumulation of undesired inorganic solid deposit at a metal−fluid phase interface. It is established that clogging is enhanced by (1) the increase in either concentration of the coprecipitating ions and (2) the application of electric field of a proper orientation. It is to be noted that both effects were demonstrated and the behavior captured in the present study. The physical alteration of deposits by electric fields has found its way to a wide variety of applications such as ceramic composites,[21] water treatment processes,[45] filters performance,[46,47] and granular flow systems.[48]

The literature is rich in studies of the effect of a magnetic field on the precipitation of calcium carbonate,[32,49−53] but the reports on the effect of an electric field on the transport properties of diffusion-precipitation reactions,[54−57] and the subsequent clogging of microsystems are scarce. Bena et al.[57] presented a generalized theory for the effect of an electric field on Liesegang systems, based on a Cahn−Hilliard description with mean field approximations.[58] The model predicts a host of field-dependent phenomena for the Liesegang bands, in both forward and reverse fields. Yu and Neretnieks[59] modeled transport and reaction processes including precipitation, electromigration, and electroosmosis in a porous medium under the influence of an external electric field. They studied the removal of copper from sand by means of an external electric field. They found that the electrode reactions can cause a steep pH jump somewhere in the porous medium. This jump constrains copper accumulation at this location. The insertion of a conductive solution next to the tube containing sand shifted the accumulation location out of the sand. Hence, the external electric field can be used to remove some components of the electrolyte out of the system and thus avoid clogging of the system by a precipitate.

References and Notes

(1) Yen, A.; Lee Koo, Y.-E.; Kopelman, R. Experimental Study of a Crossover from Nonclassical to Classical Chemical Kinetics: An Elementary and Reversible A + B ↔ C Reaction-Diffusion Process in a Capillary. *Phys. Rev. E* **1996**, *54*, 2447.

(2) Taitelbaum, H.; Vilensky, B.; Lin, A.; Yen, A.; Lee Koo, Y.-E.; Kopelman, R. Competing Reactions with Initially Separated Components. *Phys. Rev. Lett.* **1996**, *77*, 1640.

(3) López Cabarcos, E.; Chein-Shiu, Kuo; Scala, A.; Bansil, R. Crossover between Spatially Confined Precipitation and Periodic Pattern Formation in Reaction-Diffusion Systems. *Phys. Rev. Lett.* **1996**, *77*, 2834.

(4) Park, S. H.; Parus, S.; Kopelman, R.; Taitelbaum, H. Gel-Free Experiments of Reaction-Diffusion Front Kinetics. *Phys. Rev. E* **2001**, *64*, 055102(R).

(5) Baroud, Ch. N.; Okkels, F.; Ménétrier, L.; Tabeling, P. Reaction-Diffusion Dynamics: Confrontation Between Theory and Experiment in a Microfluidic Reactor. *Phys. Rev. E* **2003**, *67*, 060104(R).

(6) Lee Koo, Y.-E.; Kopelman, R. Space- and Time-Resolved Diffusion-Limited Binary Reaction Kinetics in Capillaries: Experimental Observation of Segregation, Anomalous Exponents, and Depletion Zone. *J. Stat. Phys.* **1991**, *65*, 893.

(7) Park, S. H.; Peng, H.; Kopelman, R.; Taitelbaum, H. Dynamical Localization-Delocalization Transition of the Reaction-Diffusion Front at a Semipermeable Cellulose Membrane. *Phys. Rev. E* **2007**, *75*, 026107.

(8) Gálfi, L.; Rácz, Z. Properties of the Reaction Front in an A + B → C Type Reaction-Diffusion Process. *Phys. Rev. A* **1988**, *38*, 3151–3154.

(9) Larralde, H.; Araujo, M.; Havlin, Sh.; Stanley, H. E. Reaction Front for A + B → C Diffusion-Reaction Systems with Initially Separated Reactants. *Phys. Rev. A* **1992**, *46*, 855.

(10) Barkema, G. T.; Howard, M. J.; Cardy, J. L. Reaction-Diffusion Front for A + B → ∅ in One Dimension. *Phys. Rev. E* **1996**, *53*, R2017.

(11) Sancho, J. M.; Romero, A. H.; Lindenberg, K.; Sagués, F.; Reigada, R.; Lacasta, A. M. A + B → 0 Reaction with Different Initial Patterns. *J. Phys. Chem.* **1996**, *100*, 19066.

(12) Sinder, M.; Pelleg, J. Asymptotic Properties of a Reversible A + B ↔ C (Static) Reaction-Diffusion Process with Initially Separated Reactants. *Phys. Rev. E* **2000**, *62*, 3340.

(13) Pribyl, M.; Snita, D.; Marek, M. Nonlinear phenomena and qualitative evolution of risk of clogging in a capillary microreactor under imposed electric field. *Chem. Eng. J.* **2005**, *105*, 99.

(14) *Oscillations and Traveling Waves in Chemical Systems*; Field, R., Burger, M., Eds.; Wiley: New York, 1985.

(15) *Phys. Chem. Chem. Phys.*A sepcial Issue on Nonlinear Kinetics. **2002**, *4*, 1253−1386.

(16) Avnir, D.; Kagan, M. Spatial Structures Generated by Chemical Reactions at Interfaces. *Nature* **1984**, *307*, 717.

(17) Kravchenko, V. V.; Medvinskii, A. B.; Reshetilov, A. N.; Ivanitskii, G. R. *Dokl. Akad. Nauk* **1999**, *364*, 114–116. Kravchenko, V. V.; Medvinskii, A. B.; Reshetilov, A. N.; Ivanitskii, G. R. *Dokl. Akad. Nauk* **1999**, *364*, 687–689.

(18) Ortoleva, P., *Geochemical Self-Organization*; Oxford University Press: New York, 1994.

(19) *Growth, Dissolution and Pattern Formation in Geosystems*; Jamtveit, B., Meakin, P., Eds.; Kluwer Academic Publishers: Dordrecht, 1999.

(20) Msharrafieh, M.; Al-Ghoul, M.; Sultan, R. Simulation of Geochemical Banding in Acidization-Precipitation Experiments In-Situ. In Complexus Mundi: Emergent Patterns in Nature; Novak, M. M., Ed.; World Scientific: Singapore, 2006; pp 225−236.

(21) Bao, Y.; Nicholson, P. S. Constant Current Electrophoretic Infiltration Deposition of Fiber-Reinforced Ceramic Composites. *J. Am. Ceram. Soc.* **2007**, *90*, 1063–1070.

(22) Backfolk, K.; Lagerge, S.; Rosenholm, J. The Influence of Stabilizing Agents on the Interaction between Styrene/Butadiene Latex and Calcium Carbonate: A Calorimetric and a Dynamic Electrokinetic Study. *J. Colloid Interface Sci.* **2002**, *254*, 8.

(23) Chong, T.; Sheikholeslami, R. Thermodynamics and Kinetics for Mixed Calcium Carbonate and Calcium Sulfate Precipitation. *Chem. Eng. Sci.* **2001**, *56*, 5391.

(24) Magnico, P. Impact of Dynamic Processes on the Coupling between Fluid Transport and Precipitate Deposition. *Chem. Eng. Sci.* **2000**, *55*, 4323.

(25) Hampton, J.; Savage, S. Computer Modeling of Filter Pressing and Clogging in Random Tube Network. *Chem. Eng. Sci.* **1993**, *48*, 1601.

(26) Taitelbaum, H.; Havlin, Sh.; Kiefer, J. E.; Trus, B.; Weiss, G. H. Some Properties of the A + B → C Reaction-Diffusion System with Initially Separated Components. *J. Stat. Phys.* **1991**, *65*, 873.

(27) Taitelbaum, H.; Lee Koo, Y.-E.; Havlin, Sh.; Kopelman, R.; Weiss, G. H. Exotic Behavior of the Reaction Front in the A + B → C Reaction-Diffusion System. *Phys. Rev. A* **1992**, *46*, 2151.

(28) Dee, G. T. Patterns Produced by Precipitation at a Moving Reaction Front. *Phys. Rev. Lett.* **1986**, *57*, 275.

(29) Liesegang, R. E. Chemische Fernwirkung. *Lieseg. Photograph. Arch.* **1896**, *37*, 305. continued on p 331.

(30) Henisch, H. K. *Crystals in Gels and Liesegang Rings*; Cambridge University Press: Cambridge, 1988.

(31) *Handbook of Chemistry and Physics*, 88th ed.; Lide, D. F., Ed.; CRC Press: Boca Raton, FL, 2008. $K_1 = 4.47 \times 10^{-7}$; $K_2 = 4.67 \times 10^{-11}$.

(32) Kobe, S.; Drazic, G.; Cefalas, A.; Sarantopoulou, E.; Strazisar, J. Nucleation and Crystallization of $CaCO_3$ in Applied Magnetic Fields. *Cryst. Eng.* **2002**, *5*, 243.

(33) Baroud, C. N.; Okkels, F.; Ménétrier, L.; Tabeling, P. Reaction-Diffusion Dynamics: Confrontation Between Theory and Experiment in a Microfluidic Reactor. *Phys. Rev. E* **2003**, *67*, 060104(R).

(34) Ismagilov, R. F.; Stroock, A. D.; Kenis, P. J. A.; Whitesides, G. Experimental and Theoretical Scaling Laws for Transverse Diffusive Broadening in Two-Phase Laminar Flows in Microchannels. *Appl. Phys. Lett.* **2000**, *76*, 2376.

(35) Taitelbaum, H.; Koza, Z. Anomalous Kinetics of Reaction-Diffusion Fronts. *Philos. Mag. B* **1998**, *77*, 1389–1400.

(36) Mandalian, L.; Fahs, M.; Al-Ghoul, M.; Sultan, R. Morphology, Particle Size Distribution and Composition in One- and Two-Salt Metal Oxinate Liesegang Patterns. *J. Phys. Chem. B* **2004**, *108*, 1507–1514.

(37) Kai, S.; Müller, S. C.; Ross, J. Periodic Precipitation Patterns in the Presence of Concentration Gradients. 2. Spatial Bifurcation of Precipitation Bands and Stochastic Pattern Formation. *J. Phys. Chem.* **1983**, *87*, 806–813.

(38) Havlin, S.; Araujo, M.; Larralde, H.; Stanley, H. E.; Trunfio, P. Diffusion-Controlled Reaction, A + B → C, with Initially Separated Reactants. *Phys. A* **1992**, *191*, 143.

(39) Havlin, S.; Araujo, M.; Lereah, Y.; Larralde, H.; Shehter, A.; Stanley, H. E.; Trunfio, P.; Bilensky, B. Complex Dynamics in Initially Separated Reaction-Diffusion Systems. *Phys. A* **1995**, *221*, 1.

(40) Kaprivsky, P. L. Diffusion-Limited Annihilation with Initially Separated Reactants. *Phys. Rev. E* **1995**, *51*, 4774.

(41) Hecht, I.; Moran, Y.; Taitelbaum, H. Reaction-Diffusion Front Width Anomalies in Disordered Media. *Phys. Rev. E* **2006**, *73*, 051109.

(42) Weiss, G.; Kopelman, R.; Havlin, S. Density of Nearest-Neighbor Distances in Diffusion-Controlled Reactions at a Single Trap. *Phys. Rev. A* **1989**, *39*, 466.

(43) Huang, Y.; Fowkes, F.; Lloyd, T.; Sanders, N. Adsorption of Calcium Ions from Calcium Chloride Solutions onto Calcium Carbonate Particles. *Langmuir* **1990**, *7*, 1742.

(44) Bena, I.; Coppex, F.; Droz, M.; Rácz, Z. Front Motion in an A + B → C Type Reaction-Diffusion Process: Effects of an Electric Field. *J. Chem. Phys.* **2005**, *122*, 024512.

(45) Cho, Y. I. Water Treatment Process and Apparatus. US Patent, World Intellectual Property Organization, Patent No. WO/2003/040043, 2003.

(46) Rosenberg, G., Innovative Defense Technologies Ltd., Method and Construction of Filters and Pre-Filters for Extending the Life Cycle of the Filter Bodies Therein. US Patent, World Intellectual Property Organization, Patent No. WO/2004/071613, 2004.

(47) Yang, G. C. C.; Yang, T.-Y.; Tsai, Sh.-Hi. Crossflow Electro-Microfiltration of Oxide-CMP Wastewater. *Water Res.* **2003**, *37*, 785–792.

(48) Chen., W.; Hou, M.; Jiang1, Z.; Lu, K.; Lam, L. Intermittent Granular Flow in the Presence of an Electric Field. *Europhys. Lett.* **2001**, *56*, 536–541.

(49) Chibowski, E.; Szczes, A.; Holysz, L. Influence of Sodium Dodecyl Sulfate and Static Magnetic Field on the Properties of Freshly Precipitated Calcium Carbonate. *Langmuir* **2005**, *21*, 8114.

(50) Holysz, L.; Chibowski, M.; Chibowski, E. Time-Dependent Changes of Zeta Potential and Other Parameters of In Situ Calcium Carbonate due to Magnetic Field Treatment. *Colloids Surf., A* **2001**, *208*, 231.

(51) Azuma, N.; Tajima, K.; Ishizu, K.; Yokoi, I.; Mori, A. Detection and a Possible Mechanism of Magnetic Field Effect on the Crystal Growth of Sedimentary Calcium Carbonate. *Pathophysiology* **2000**, *7*, 83.

(52) Higashitani, K.; Kage, A.; Katamura, S.; Imai, K.; Hatade, S. Effects of a Magnetic Field on the Formation of $CaCO_3$ Particles. *J. Colloid Interface Sci.* **1993**, *156*, 90.

(53) Chibowski, E.; Holysz, L.; Terpilowski, K. Effect of magnetic field on deposition and adhesion of calcium carbonate particles on different substrates. *J. Adhes. Sci. Technol.* **2003**, *17*, 2005.

(54) Sultan, R.; Halabieh, R. Effect of an Electric Field on $Co(OH)_2$ Liesegang Patterns. *Chem. Phys. Lett.* **2000**, *332*, 331.

(55) Sultan, R.; Al-Ghoul, M. Front Propagation in Patterned Precipitation 2. Electric Effects in Precipitation-Dissolution Patterning Schemes. *J. Phys. Chem. A* **2003**, *107*, 1095.

(56) Shreif, Z.; Mandalian, L.; Abi-Haydar, A.; Sultan, R. Taming Ring Morphology in 2D $Co(OH)_2$ Liesegang Patterns. *Phys. Chem. Chem. Phys.* **2004**, *6*, 3461.

(57) Bena, I.; Droz, M.; Rácz, Z. Formation of Liesegang Patterns in the Presence of an Electric Field. *J. Chem. Phys.* **2005**, *122*, 204502.

(58) Cornell, S.; Droz, M. Steady-State Reaction-Diffusion Front Scaling for mA + nB → [inert]. *Phys. Rev. Lett.* **1993**, *70*, 3824.

(59) Yu, J.; Neretnieks, I. Modeling of Transport and Reaction Processes in a Porous Medium in an Electric Field. *Chem. Eng. Sci.* **1996**, *51*, 4355.

JP8087226